

## Full Length Article

# Identification of a novel binding inhibitor that blocks the interaction between hSCARB2 and VP1 of enterovirus 71

Qi Tang<sup>a,b</sup>, Zhichao Xu<sup>d</sup>, Fan Zhang<sup>b</sup>, Yang Cai<sup>b</sup>, Yinuo Chen<sup>b</sup>, Baojing Lu<sup>a</sup>, Hai-bing Zhou<sup>d,e</sup>, Ke Lan<sup>b,c,\*</sup>, Shuwen Wu<sup>b,\*\*</sup>

<sup>a</sup> Department of Microbiology, The Key Laboratory of Microbiology and Parasitology of Anhui Province, The Key Laboratory of Zoonoses of High Institutions in Anhui, School of Basic Medical Sciences, Anhui Medical University, Hefei, China

<sup>b</sup> State Key Laboratory of Virology, College of Life Sciences, Wuhan University, Wuhan, 430071, China

<sup>c</sup> Medical Research Institute, Wuhan University, Wuhan, 430071, China

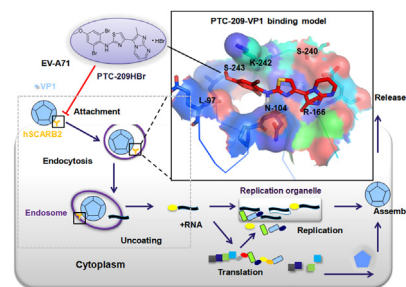
<sup>d</sup> Hubei Provincial Key Laboratory of Developmentally Originated Disease, Hubei Province Engineering and Technology Research Center for Fluorinated Pharmaceuticals, Wuhan University School of Pharmaceutical Sciences, Wuhan, 430071, China

<sup>e</sup> Medical Research Institute, Frontier Science Center for Immunology and Metabolism, Wuhan University, Wuhan, 430071, China

## HIGHLIGHTS

- PTC-209HBr and its derivatives inhibited multiple enteroviruses with an EC<sub>50</sub> at the submicromolar level.
- Mechanism studies showed PTC-209HBr suppressed EV-A71 by blocking the interaction between hSCARB2 and VP1.
- VP1 N104S and S243P et al., mutants were identified by resistance and fitness study.
- N104S mutant could enhance the fitness of EV-A71 by increasing the interaction between VP1 and hSCARB2 in the presence of PTC-209HBr.

## GRAPHICAL ABSTRACT



## ARTICLE INFO

**Keywords:**  
EV-A71  
Enterovirus  
DAAs  
VP1  
PTC-209HBr  
Pirodavir  
Enviroxime  
hSCARB2

## ABSTRACT

Enterovirus 71 (EV-A71) infection causes severe hand-foot-and-mouth disease that leads to cardiopulmonary complications and death in young children under 5 years of age. Although there are available vaccines for EV-A71 C<sup>4</sup>, however, there are no efficient drugs for severe cases. Thus, there is an urgent need to find new direct-antiviral agents (DAAs) to control EV-A71 infection. In this study, we report our discovery of the EV-A71 capsid inhibitor PTC-209HBr, a small-molecule Bmi-1 inhibitor and an anticancer agent, and its derivatives that inhibit multiple enteroviruses with an EC<sub>50</sub> at a submicromolar efficacy. The mechanism of action of PTC-209HBr was confirmed by time-of-addition, resistance selection and reverse genetics experiments, microscale thermophoresis (MST), viral binding and entry assays, coimmunoprecipitation (Co-IP) and immunofluorescence experiments (IF). Mechanistic studies indicated that PTC-209HBr inhibited EV-A71 infection by impeding the binding between VP1 and the receptor hSCARB2 during the early stage of EV-A71 infection through hindering viral entry into host cells. Collectively, these findings indicated that PTC-209HBr is a novel inhibitor of enteroviruses with a confirmed mechanism of action that can be further developed into EV-A71 DAAs.

\* Corresponding author. State Key Laboratory of Virology, College of Life Sciences, Wuhan University, Wuhan, 430071, China.

\*\* Corresponding author.

E-mail addresses: [klan@whu.edu.cn](mailto:klan@whu.edu.cn) (K. Lan), [shuwenwu@whu.edu.cn](mailto:shuwenwu@whu.edu.cn) (S. Wu).

<https://doi.org/10.1016/j.cellin.2022.100016>

Received 11 October 2021; Received in revised form 13 January 2022; Accepted 8 February 2022

Available online 12 February 2022

2772-8927/© 2022 Wuhan University. Published by Elsevier B.V. on behalf of Wuhan University. This is an open access article under the CC BY-NC-ND license (<http://creativecommons.org/licenses/by-nc-nd/4.0/>).

## 1. Introduction

Hand, foot and mouth disease (HFMD), which is a common disease among people in the Asia-Pacific region, especially in young children, is generally considered to be caused by enteroviruses (EVs) (Chang et al., 1999; Yang et al.). Since EV-A71 was first isolated from an infant with encephalitis in California in 1969, it has spread around the world (Baggen et al., 2018). In the autumn of 2008, there was an outbreak of HFMD caused by CV-A6 in Finland (Osterback et al., 2009). Singapore suffered its largest ever outbreak of HFMD in 2008, which resulted in 29,686 infections, including four cases of encephalitis and one death (Wu et al., 2010). In China, between 2009 and 2011, more than half a million large-scale outbreaks of hand, foot and mouth disease were reported every year. In 2010, China suffered the worst outbreak of HFMD associated with enterovirus 71 (EV-A71), with more than 1.7 million cases, 27,000 cases of severe neurological complications and 905 deaths (Zeng et al., 2012). The disease broke out in Thailand in 2012, infecting more than 39,000 people (Linsuwanon et al., 2014). Among the 13 species of enteroviruses, two serotypes from the A species, EV-A71 and coxsackievirus 16 (CV-A16), are the main pathogens for HFMD (Yang et al., 2017). EV-A71 causes a lower incidence of HFMD than CV-A16, but because EV-A71 is a neurotropic virus, it leads to more severe symptoms (Yang et al., 2017). Typical symptoms of HFMD are fever, skin eruptions on hands and feet, and vesicles in the mouth, but in disease associated with EV-A71, patients may rapidly develop fatal neurological and systemic complications including aseptic meningitis, encephalitis, acute flaccid paralysis, and myocarditis (Chang et al., 1999; Xing et al., 2014). The neurotropic nature of EV-A71 also makes it more lethal such that more than 90% of deaths from HFMD are related to EV-A71 (Xing et al., 2014). In Asia-Pacific countries, mortality rates due to EV-A71 infection ranged from less than 0.5%–19% (Linsuwanon et al., 2014). Widespread infection and possible death precipitate the need for the development of effective drug therapies.

EV-A71 is a member of the *Picornaviridae* family, genus *Enterovirus*. The EV-A71 particle is a nonenveloped icosahedral and 20–30 nm in diameter (Chang et al., 1999). Its genome is a single-strand positive-sense RNA consisting of 7500 nucleotides, which translates into a large polyprotein that is cleaved into 3 regions: P1, P2, and P3. The P1 region encodes four capsid proteins: VP1, VP2, VP3, and VP4. The P2 and P3 regions encode nonstructural proteins, such as proteases and RNA polymerases (Huang et al., 2009). Sixty protomers, each of which consists of VP1 to VP4, are assembled to form a capsid (Plevka et al., 2012). VP1 to VP3 are on the surface of the viral capsid and are therefore easily recognized as antigens, whereas VP4 is inside the viral capsid (Rossmann et al., 2002). EV-A71 binds to host cells via the human scavenger receptor B2 (hSCARB2), P-selectin glycoprotein ligand (PSGL-1), sialylated glycans, heparin sulfate, annexin A2, and heat shock protein 90 (Baggen et al., 2018; Hu et al., 2020). Due to the low pH of the endosome, it is enclosed, and the capsid deforms and converts into “A-particles”, lacking the internal capsid protein VP4 and exposing N-terminal amphipathic sequences of VP1, which is conducive to direct interaction between VP1 and the lipid bilayer (Tosteson and Chow, 1997). The uncoated viral RNA is then released through a pore in the endosome into the cytoplasm; subsequently, protein translation and viral replication begin (Lee et al., 2017). Functionally speaking, VP1 not only plays a crucial role in attachment and penetration but also induces autophagy in neuronal cells to facilitate viral replication (Wen et al., 2021); in terms of antigenicity, VP1 contains the major neutralization epitopes, and allows for EV-A71 molecular genotyping and epidemiological monitoring (Solomon et al., 2010). As a result, many studies on vaccines or antiviral reagents against EV-A71 have focused on VP1 (Hu et al., 2020; Anasir et al., 2021; Wang et al., 2021).

EV-A71 is mainly divided into three genotypes: A, B (B1–B5) and C (C1–C5). Mutations from B to C or C to B can be frequent. The most common types in China, are EV-A71-C4, CV-A6, CV-A10 and CV-A16 (Huang et al., 2009). Therefore, a broad-spectrum agent against EV-A71 and CV that causes HFMD is needed. Although EV-A71 vaccine

candidates have been developed including formalin-inactivated virions, recombinant virus-like particles, recombinant VP1, and synthetic peptides containing the EV-A71 neutralization epitope, however, there is no effective HFMD vaccine that can elicit strong cross-neutralizing antibody responses against different types of both EV-A71 and CV (Chong et al., 2015). Here, we hypothesize that anti-EV-A71 antibodies failed to cross-neutralize CV-A16 due to their amino acid sequence dissimilarity. In addition to using vaccines to prevent and treat HFMD, there is also great potential to develop antiviral agents. As the understanding of the structure and infection process of EV-A71 increases, and due to computer-assisted drug design technology evolving, the development of new broad-spectrum anti-EV-A71 drugs has attracted much attention.

There are two main types of antiviral agents, and one type is virus-targeted antiviral drugs that directly or indirectly inhibit the biological activity of viral proteins. For example, pleconaril is one of the capsid binding compounds targeted at VP1 among the WIN antivirals, which has an inhibitory effect on most enteroviruses and rhinoviruses (Fleischer and Laessig, 2003; Lou et al., 2014). MADAL385 prevents the virus from interacting with PSGL1 and heparin sulfate by interacting with each vertex on the capsid, thus blocking attachment (Sun et al., 2019). Pyridyl imidazolidinones, pirodavidir, and vapendavidir are inhibitors of EV-A71 that target a hydrophobic pocket formed by VP1 to inhibit virus adsorption or uncoating in the early stages of its replication (Shia et al., 2002; Tijjsma et al., 2014). By inhibiting viral 3A or 3D polymerase, aurintricarboxylic acid, NITD008, FNC, gemcitabine and ribavirin suppress enterovirus replication (Kang et al., 2015; Baggen et al., 2018). Emetine and prunin are broad-spectrum inhibitors of EV acting on the internal ribosomal entry site (IRES) with both *in vivo* and *in vitro* antiviral activity (Gunaseelan et al., 2019). The other type of antiviral agent are host-targeted antiviral drugs targeting host cell factors involved in the life cycle of enteroviruses: Itraconazole, enviroxime and geldanamycin are a class of anti-enterovirus inhibitors that target host factors OSBP, PI4KB and HSP90, respectively (Baggen et al., 2018). However, there are currently no approved antiviral drugs for EV-A71 or any other enterovirus (Lin et al., 2019).

In this study, we applied a high-throughput screening (HTS) assay to screen more than 12,000 compounds and initially identified PTC-209HBr, a small-molecule Bmi-1 inhibitor and an anticancer agent, as an EV-A71 inhibitor. Hopcraft et al. previously reported that PTC-209HBr as a novel inhibitor of a member of the polycomb repressive complex 1, Bmi1, stimulates KSHV reactivation from latency by altering histone modifications and nucleosome density at the RTA promoter (Hopcraft et al., 2018). However, the roles and molecular mechanism of PTC-209HBr inhibition of enteroviruses are unknown. Here, time-course assay, binding and entry assays showed that PTC-209HBr effectively inhibited EV-A71 infection by blocking adsorption or uncoating in the early stages in the early stage. Furthermore, PTC-209HBr was used to screen and identify the drug-resistant virus, and sequence analysis showed that two mutation sites: A2747G (VP1 N104S) and T316C (VP1 S243P). Among them, compared to untreated viruses, only the N104S and S243P variants could significantly resist to PTC-209HBr. MST assay results indicated that PTC-209HBr and VP1 may interact directly. The Immunofluorescence (IF) and coimmunoprecipitation (Co-IP) results indicated that PTC-209HBr may target the EV-A71 capsid protein VP1 and impede the binding between VP1 and the receptor. Overall, our study presents a confirmed mechanism of action for PTC-209HBr and provides a potential agent that be further developed into EV-A71 antivirals.

## 2. Materials and Methods

### 2.1. Cell lines, antibodies, viruses, plasmids and compounds

RD cells, HeLa cells, HEK293T cells and Vero cells were purchased from ATCC (USA). An anti-EV-A71 VP1 antibody (10F0) and a mouse anti-tubulin mAb (T5168) used in Western blot or IF analysis were

purchased from Abcam, GeneTex, Merck or Sigma. An anti-SCARB2 (A9185) poly-antibody and an anti-KENMEN1 (A10507) were purchased from ABclonal, respectively. EV71/HeN09, Echov-6, CV-A16, CV-B1, CV-B3, CV-B6 and EV-D68 were provided by the State Key Laboratory of Virology, College of Life Sciences, Wuhan University and used as previously described. EV-A71 GZ-CII and EV71/G082 was kindly provided by Dr Tao Peng (Guangzhou, China) and Dr. Zhong Huang (Shanghai, China) (Xu et al., 2017). pACYC-EV71-FL was provided by Dr Bo Zhang (Wuhan, China) (Shang et al., 2013; Xia et al., 2015). An FDA-approved drug library (L1300) and the clinical compound library (L3900) and the library of pharmacologically active compounds Sigma (LO2219) were purchased as previously reported (Tang et al., 2020a). PTC-209HBr, pirodavir and enviroxime were purchased from Selleck (S7539), Targetmol (T1750) and MedKoo (319912), respectively.

## 2.2. HTS

An HTS assay based on the cytopathic effect (CPE) was performed as previously reported (Tang et al., 2020a). Briefly, RD cells were infected with EV-A71 at a multiplicity of infection (MOI) of 0.1, followed by the treatment of compounds (10  $\mu$ M). The antiviral activities of compounds were measured by a CCK8 kit based on cell viability. The antiviral effect of potential compounds was further assessed by western blotting. The cytotoxic effect was tested by a CCK-8 kit (Vazyme Biotech) as previously reported and the selective index (SI) was calculated based on the EC<sub>50</sub>/CC<sub>50</sub> values.

## 2.3. Short-term treatment assay for assessment of compound sensitivity

In concentration-response experiments, a CPE assay or qRT-PCR assay was conducted to assess compound sensitivity. In short, infected RD cells were treated with a dilution series of PTC-209HBr, pirodavir or enviroxime at 1 h postinfection (hpi), and single infected cells were counted at 24 hpi. For relative viral RNA levels, the determination of viral RNA levels was performed as previously reported, and GAPDH was used as the standard to quantify relative viral RNA accumulation (Tang et al., 2020a).

## 2.4. Plaque assay

A plaque assay was performed as previously reported (Baer and Kehn-Hall, 2014). In short, RD cells were infected with diluted viruses, then treated with a mixture of 2 $\times$  MEM and 1% low gelling temperature agarose at 1 hpi. Finally, samples were fixed with 4% paraformaldehyde, stained by 1% crystal violet and the calculation of EC<sub>50</sub> values was carried out with GraphPad Prism 8.0 based on nonlinear regression, as previously described (Jensen et al., 2019).

## 2.5. Cytotoxicity assay

Cell proliferation and cytotoxicity were determined by a CCK8 kit (Vazyme Biotech) according to the manufacturer's instructions. GraphPad Prism 8.0 was used to calculate the CC<sub>50</sub>, as previously reported (Tang et al., 2020a).

## 2.6. Time-of-addition assay

PTC-209HBr (3.20  $\mu$ M), enviroxime (0.60  $\mu$ M) or pirodavir (1.44  $\mu$ M) was added to RD or Vero cell cultures at the indicated time points (0, 1, 2, 4, 6, and 8 h) before or after infection with EV-A71 at an MOI of 0.1, as previously reported (Tang et al., 2020a). Samples were harvested at 12 hpi, and total RNA and cell lysates were collected. Viral RNA accumulation and viral protein expression were determined by qRT-PCR (primers listed in Table 1) and Western blot, respectively. The viral protein VP1 was assessed by Western blot analysis. The visualization and quantification of western blots were carried out with an Amersham Imager 600 (GE Healthcare).

## 2.7. Western blot analysis and CO-IP

The Western blot assay protocol was described in a previous study (Tang et al., 2020b). In short, samples were lysed with cold RIPA buffer at 4  $^{\circ}$ C for 1 h and then were boiled at 100  $^{\circ}$ C for 10 min with 2 $\times$  SDS loading buffer, followed by electrophoresis by sodium dodecyl sulfate (SDS) polyacrylamide gel electrophoresis (PAGE). The separated proteins were then transferred onto the nitrocellulose (NC) membranes. The NC membrane containing proteins was incubated with anti-VP1 (1:4000) in

**Table 1**  
Oligonucleotides used in this study.

Primers	Primer sequence (5' - 3')	Purpose
qEV71 PCR-F	TGAATGCGGCTAATCCCAACT	qRT-PCR
qEV71 PCR-R	AAGAAACACGGACACCCAAAG	qRT-PCR
qGAPDH PCR-F	CCCACCTCCTCCACCTTTGACG	qRT-PCR
qGAPDH PCR-F	CACCACCCTGTTGCTGTAGCCA	qRT-PCR
A2747G(N104S)-F	AACCCAAgTGGTTATGCCAACTGGGACATAGA	Generate mutant virus
A2747G(N104S)-R	GCATAACCAcTTGGGTTAGTTGTGCCCTCAAAG	Generate mutant virus
T3163C(S243P)-F	CCTCCAAGcCCAAGTATCCTTTAGTGGTTAGGATTT	Generate mutant virus
T3163C(S243P)-R	ATACTTGgCTTGGAGGTCCCCACAGTCCGCA	Generate mutant virus
A2741G(N102S)-F	CACAACtAgCCCAATGGTTATGCCAACTGGG	Generate mutant virus
A2741G(N102S)-R	CATTTGGGcTAGTTGTGCCCTCAAGAGGGAGA	Generate mutant virus
A2632G(T66A)-F	TGATTGAGgCACGCTGTGTTCTCAACTCGCAC	Generate mutant virus
A2632G(T66A)-R	ACAGCGTgCtCAATCATGCTCTCGTCACTAGC	Generate mutant virus
G2780A(R121K)-F	CGGTAAaAAGGTAGAGCTATTACCTACATGC	Generate mutant virus
G2780A(R121K)-R	GCTCTACCTTTtACGCATTTGGCGGTAACCT	Generate mutant virus
VP1-EGFP-F	CCAAGCTTATGGGAGATAGGGTGGCAGATGTAATTG	Generate VP1 protein
VP2-EGFP-R	CGGGATCC CG AAGAGTGGTGATCGCTGTGCGAC	Generate VP1 protein
VP1-EGFP N104S-F	AACCCAAgTGGTTATGCCAACTGGGACATAGA	Generate mutant VP1 protein
VP1-EGFP N104S-R	GCATAACCAcTTGGGTTAGTTGTGCCCTCAAAG	Generate mutant VP1 protein
VP1-EGFP S243P-F	CCTCCAAGcCCAAGTATCCTTTAGTGGTTAGGATTT	Generate mutant VP1 protein
VP1-EGFP S243P-R	ATACTTGgCTTGGAGGTCCCCACAGTCCGCA	Generate mutant VP1 protein
hSCARB2-EGFP-F	CGCTCGAGATGGGCCGATGCTGCTTCTACAC	Generate EGFP-hSCARB2 protein
hSCARB2-EGFP-R	CCGGAATCCGGGTTCCGAATGAGGGGTGCTC	Generate EGFP-hSCARB2 protein
Flag-VP1-F	CCAAGCTTgCCCACTGGGAGATAGGGTGGCAGATGTAATTG	Generate Flag-VP1 protein
Flag-VP1-R	CGGGATCCaAGAGTGGTGATCGCTGTGCGAC	Generate Flag-VP1 protein
HA-hSCARB2-F	CGGAATTCGGATGGGCCGATGCTGCTTCTACAC	Generate HA-hSCARB2 protein
HA-hSCARB2-R	CCGCTCGAGTTAGTTTCCGAATGAGGGGTGCTC	Generate HA-hSCARB2 protein

1× PBS overnight at 4 °C and subsequently stained with secondary antibodies for 1 h at room temperature. Finally, western blots were visualized and quantified using an Amersham Imager 600 (GE Healthcare).

## 2.8. Immunofluorescence assay

The IF assay protocol was described in a previous study (Tang et al., 2020b). Briefly, cell samples were fixed with 4% paraformaldehyde for 30 min and then permeabilized with 0.1–0.5% Triton X-100 in PBS for 10 min. Cells were incubated with an anti-VP1(1:2000) or a LIMP2 (hSCARB2) polyclonal antibody or KREMEN1 polyclonal antibody in 1× PBS overnight at 4 °C and subsequently stained with secondary antibodies for 1 h at room temperature and then incubated with a 4',6-diamidino-2-phenylindole (DAPI) solution (Beyotime, C1002) for 5 min at room temperature. Finally, the cells were visualized and quantified with a Leica confocal microscope.

## 2.9. Generation of PTC-209HBr-resistant viruses

PTC-209HBr resistance profiling was carried out as previously reported. Briefly, RD cells were infected with EV-A71 virus and treated with 1- to 4-fold EC<sub>50</sub> of PTC-209HBr. Escaped viruses emerged during long-term treatment with PTC-209HBr. Sanger sequencing was applied to identify the sequences of escaped viruses, and the mutations in VP1 was further identified by a subclone assay. In short, viral RNA of resistant viruses was extracted from the supernatant by a High Pure Viral Nucleic Acid Kit (Roche Kit), followed by an inverse transcription PCR (SuperScript™ III, Invitrogen). Eight amplicons, which covered the full length of EV-A71 genome and produced by a nest PCR assay from the cDNA, were sequenced. As for the subclone assay, only the full length of VP1 was amplified from the amplicons, followed by a TA clone assay. Finally, ten clonal samples were sequenced and identified. Then resistance-associated mutations were engineered for a resistance study. A Mut Express II Fast Mutagenesis Kit V2 (Vazyme Biotech) or QuikChange Site-Directed Mutagenesis Kit (Agilent) was used to introduce mutations in the wild type (WT). The primers for engineering mutations are listed in Table 1. The mutant viral genome sequences were all confirmed by Sanger sequencing (Sangon Biotech) and subclone analysis.

## 2.10. EV-A71 sequence analysis

For EV-A71 sequence analysis, EV-A71 RNA was extracted from cell culture supernatants, followed by cDNA synthesis (Tang et al., 2014). The entire genome was cloned into eight amplicons and then identified by Sanger sequencing (Sangon Biotech). The primers for these amplicons were previously described (Tang et al., 2020a). Sequence analysis was performed with Sequencher (GeneCodes) as previously reported (Pham et al., 2019).

## 2.11. Binding and entry assay

For the binding assay, the indicated doses of PTC-209HBr, enviroxime or pirodavir were mixed with EV-A71 (30 MOI) before attachment to DMEM containing 2% FBS. After incubation at 37 °C for 1 h, the mixtures were added to RD or Vero cells cultured in 12-well plates and followed by incubation at 4 °C for 1 h to allow virus attachment. To remove unbound viruses, cells were washed five times with cold PBS before collection. Finally the cells were harvested and analyzed at 4 hpi or 0 hpi by Western blot or qRT-PCR assay. For the viral entry assay, RD or Vero cells were infected with EV-A71 at an MOI of 30 and then were incubated at 4 °C for 1 h to allow virus attachment. After the attachment, RD or Vero cells were washed five times with cold PBS, and then were treated with various concentrations of PTC-209HBr, enviroxime and pirodavir at 37 °C for 2 h, and finally washed five times with cold PBS. The samples were collected and analyzed by western blotting or qRT-PCR at 4 hpi and 2 hpi, respectively.

To determine the inhibitory effect of PTC-209HBr on the binding between VP1 and receptors, an IF assay was carried out to investigate the efficacy of PTC-209HBr. In short, samples were treated under the same conditions as the binding assay, followed by incubation at 37 °C for 6 h. Then, samples were harvested and analyzed by an IF assay.

## 2.12. Construction of VP1 and hSCARB2 expression vectors

The hSCARB2 construct was amplified from an RD cell cDNA library and inserted into the pCMV-HA vector at the *EcoRI* and *XhoI* sites. The VP1 coding sequence was amplified from a full-length EV-A71 infectious clone plasmid (pACYC-EV71-FL), and cloned into the pCDH-Flag (pCDH) vector at the *HindIII* and *BamHI* sites, and further subcloned into the expression vector pEGFP-N1 at the *HindIII* and *BamHI* sites. Then, the pEGFP-N1-VP1 plasmid was used to construct the VP1 N104S and VP1 S243P mutant expression plasmids with a Mut Express II Fast Mutagenesis Kit V2 (Vazyme Biotech) or QuikChange Site-Directed Mutagenesis Kit (Agilent) according to the manufacturer's instructions. All these constructs were verified by DNA sequencing (Sangon Biotech). The PCR primers used in this study are presented in Table 1.

## 2.13. MST assay

To investigate whether PTC-209HBr binds to VP1, an MST assay was carried out to determine the binding affinities between VP1 and the compounds. Compounds were diluted to the indicated concentrations and mixed with VP1-EGFP in assay MST buffer containing 0.05% Tween 20. Then, the mixed samples were loaded into Monolith NT.115 capillaries, and thermophoresis was analyzed by a Monolith NT.115 instrument (NanoTemper Technologies). The thermophoresis parameters were set as blue excitation with a power at 20% in LED, "medium" in MST power and an optimized time setting (2.5 s, MST on) as reported (Entzian and Schubert, 2016). GraphPad Prism 8 software was used out to calculating  $K_d$  value by fitting the MST data.

## 2.14. Molecular modeling

To predict the binding model between PTC-209HBr and VP1, AutoDock software was used to dock PTC-209HBr into the structure of the EV-A71 VP1 protein. The calculation of the minimal energy of PTC-209HBr and the PDB format of PTC-209HBr was carried out with Chem3D Pro 14.0. The box parameters were set as 100 Å, 100 Å, and 120 Å in the X, Y and Z dimensions, respectively, for the docking. Pretreatment of the crystal structure of the EV-A71 VP1 protein (PDB ID: 3ZFF) was carried out with PyMOL before docking as previously reported (Yu et al., 2018). Finally, PyMOL was used to perform complex analysis and figure visualization as previously reported (Han et al., 2016; Yu et al., 2018).

## 2.15. Statistical analyses

Statistical analyses were conducted using GraphPad Prism 8.0. Data are reported as the means and standard error of the means (SEMs) of the results from at least two or three independent experiments performed in triplicate. Two-tailed p values < 0.05 (\*) and 0.01 (\*\*) or 0.001 (\*\*\*) were considered statistically significant and highly significant, respectively. "ns" indicates nonsignificant differences.

## 3. Results

### 3.1. Drug repurposing screen to identify active compounds that block EV-A71

To screen the potential compounds that inhibit EV-A71 proliferation, an HTS assay was conducted to preliminarily identify the compounds that were measured by CPE. From the results of the HTS assay, we found that PTC-209 (12th) and PTC-209HBr (14th) could significantly suppress

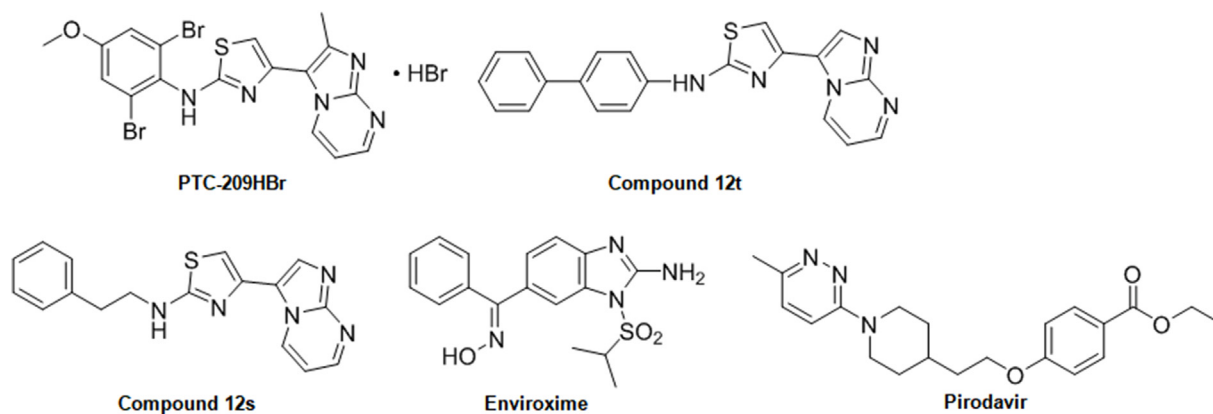


Fig. 1. Structure of EV-A71 inhibitors, PTC-209HBr and derivatives.

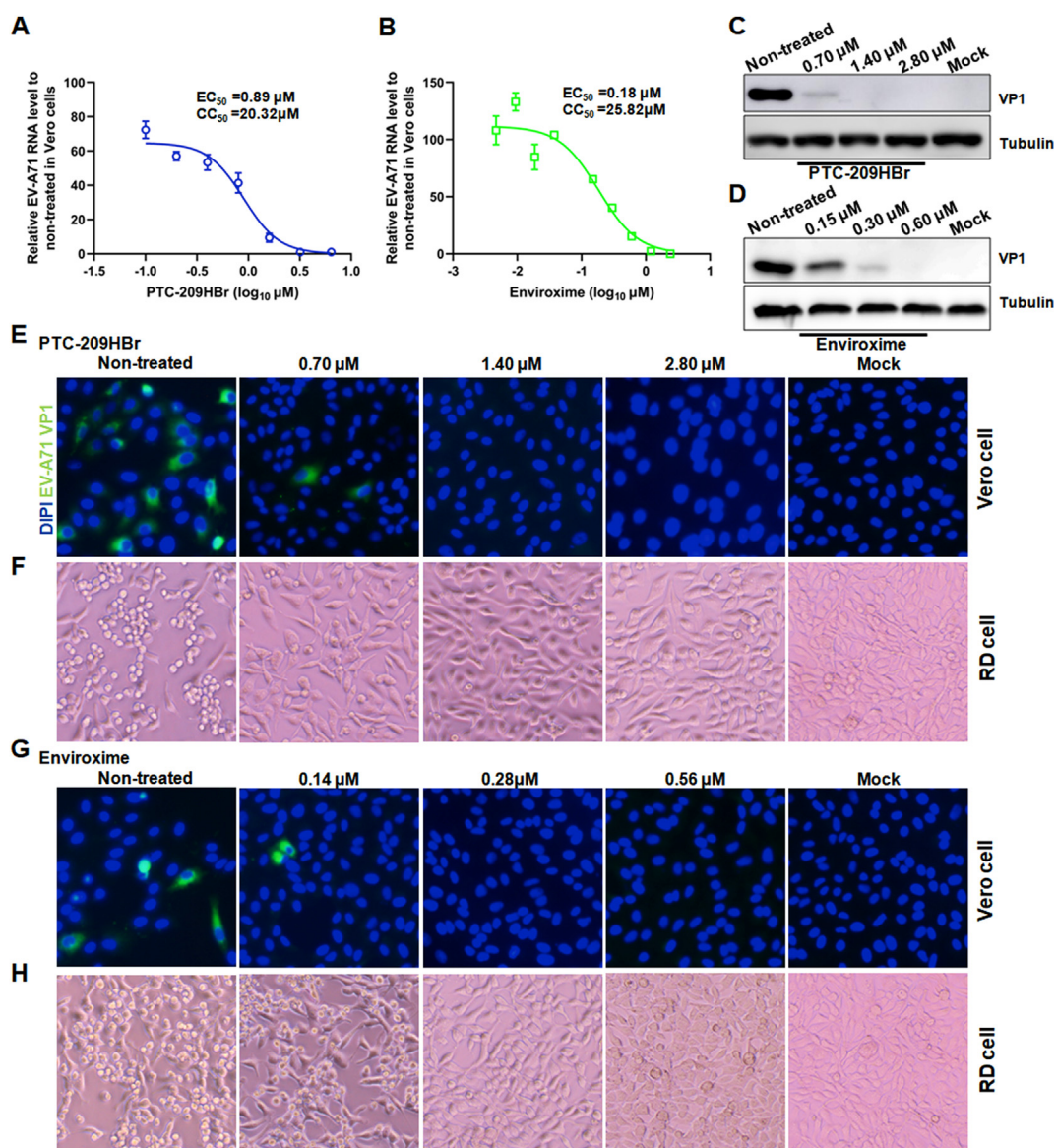


Fig. 2. Antiviral effect of PTC-209HBr and enviroxime *in vitro*. (A–H) PTC-209HBr or enviroxime significantly inhibited viral RNA level accumulation; viral protein expression and robustly impeded viral-caused CPE. Vero or RD cells were pretreated with EV-A71 at an MOI of 0.1 and then cells were incubated at 4 °C for 1 h, followed by treatment of the indicated concentration of PTC-209HBr or enviroxime for 24 h at 1 hpi. Relative viral RNA levels and protein levels in dose-dependent manner were analyzed by qRT-PCR (A, B) and Western blot (C, D), respectively. Further antiviral efficacy of PTC-209HBr against EV-A71 was tested by IF in Vero cells (E) and a CPE assay in RD cells (F). Further antiviral effects of enviroxime against EV-A71 were tested by IF in Vero cells (G) and CPE assay in RD cells (H).

the CPE caused by EV-A71 infection as previously reported (Tang et al., 2020a). The structure of PTC-209HBr and the selected control of EV-A71 inhibitors in this study are shown in Fig. 1. To further confirm the inhibitory effect of PTC-209HBr, qRT-PCR, Western blot, IF and CPE assays were conducted to measure the expression of viral RNA and the structural protein VP1, and the viral proliferation in the presence of PTC-209HBr. qRT-PCR results indicated that PTC-209HBr could inhibit the viral RNA accumulation with an EC<sub>50</sub> value of 0.89 μM (Fig. 2A) and a low CC<sub>50</sub> value at 20.32 μM (sFig 1A), and a mild SI value (22.8). The Western blot and IF results showed that PTC-209HBr, an anticancer agent, could dramatically inhibit the abundance of VP1 in dose-dependent manner (Fig. 2C, E). To test the antiviral effect on viral proliferation, a CPE assay was further conducted to analyze the *in vitro* efficacy of PTC-209HBr. The CPE assay results showed that PTC-209HBr (Fig. 2F) and its derivatives 12t/12s (sFig 1B) significantly inhibited EV-A71 proliferation, and the positive control pirodavar (sFig 1B), a VP1 inhibitor, and enviroxime, a 3A inhibitor, inhibited with EV-A71 with EC<sub>50</sub> values of 5.25 μM and 0.178 μM (Fig. 2B), respectively. Those above results PTC-209HBr could significantly inhibit viral protein expression, RNA replication and proliferation directly or indirectly. To investigate its broad antiviral efficacy, we tested PTC-209HBr against a representative species of enterovirus in a CPE assay. The results showed that PTC-209HBr exerted broad-spectrum antiviral activity with EC<sub>50</sub>s, which were between 0.796 and 2.918 μM (Fig. 3A and B). Pirodavar, a capsid inhibitor, exerted antiviral effect against selected enteroviruses at EC<sub>50</sub> values between 0.074 and 5.746 μM (sFig. 2A, 2B). Enviroxime, a 3A and PI4KB inhibitor, exhibited antiviral against selected enteroviruses examined at EC<sub>50</sub> values between 0.051 and 0.312 μM (Fig. 3A and C). These data showed that PTC-209HBr exhibited broad-spectrum of antiviral activity against enteroviruses.

### 3.2. Selection, identification, and characterization of PTC-209HBr resistance

To investigate the potential mechanism of action of PTC-209HBr, a resistance assay was conducted to identify the interactions between PTC-209HBr and viral proteins. For PTC-209HBr resistance profiling, EV-A71-

infected RD cells were treated with 2- to 4-fold EC<sub>50</sub> of PTC-209HBr. In RD cell cultures, viruses escaped after treatment with 2-fold and 4-fold PTC-209HBr in the 8th passage (Fig. 3A). To analyze the resistance profiling of escaped viruses, Sanger sequencing analysis and subclone assays were carried out to identify resistance-associated mutations. The VP1 mutations A2747G (N104S) and T316C (S243P) and one noncoding mutation C2416T in VP3 were identified by Sanger sequencing and subclone assay (Fig. 4A). Amino acids T66A, N102S, N104S, R121K and S243P were further identified in the escaped viruses by a subclone assay (Fig. 4A). The sensitivity to PTC-209HBr of mutants with amino acids N104S or S243P was tested by a CPE assay. The results showed that the sensitivity of PTC-209HBr to S243P mutant was dramatically reduced, and the EC<sub>50</sub> value for S243P was 3.56 μM (Fig. 4B and C); The sensitivity of PTC-209HBr to N104S mutant fell by about 58 percent, and the EC<sub>50</sub> value for N104S was 1.53 μM (Fig. 4B and C). Plaque assay results showed that the sensitivity of PTC-209HBr to mutants was less than that of WT in the presence of PTC-209HBr (3.56 μM) (Fig. 4D). These results indicated that the N104S and S243P mutations are important determinants of PTC-209HBr resistance and that VP1 is a potential target of PTC-209HBr in anti-enterovirus infection.

### 3.3. Binding affinity of PTC-209HBr and its derivatives with EV-A71 VP1 and VP1 mutants

To investigate whether PTC-209HBr or its derivatives bind to VP1, an MST assay was carried out to determine the binding affinity between PTC-209HBr, derivatives and VP1 or VP1 mutants. The MST assay is a biophysical technique that determines variations in the fluorescence signal as a result of an IR laser-induced temperature change, which depends on a variety of molecular properties, including size, charge, hydration shell, and conformation. The binding isotherms obtained by plotting the difference in normalized fluorescence against increasing PTC-209HBr concentration are shown in Fig. 5A. The binding affinity value of EV-A71 VP1 with PTC-209HBr was 0.245 μM. In line with the resistance results, the binding affinity of PTC-209HBr with mutant VP1 N104S ( $K_d$ :3.11 μM) and S243P ( $K_d$ :51.8 μM) was dramatically decreased that of WT VP1 as well as the derivant 12s (Fig. 5B). Interesting, there

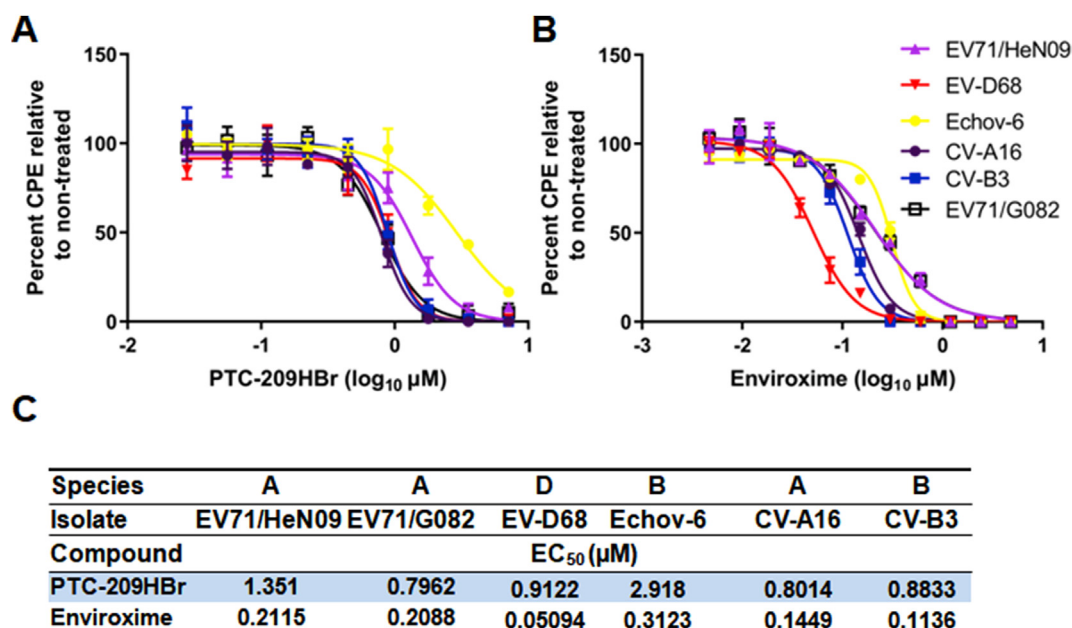
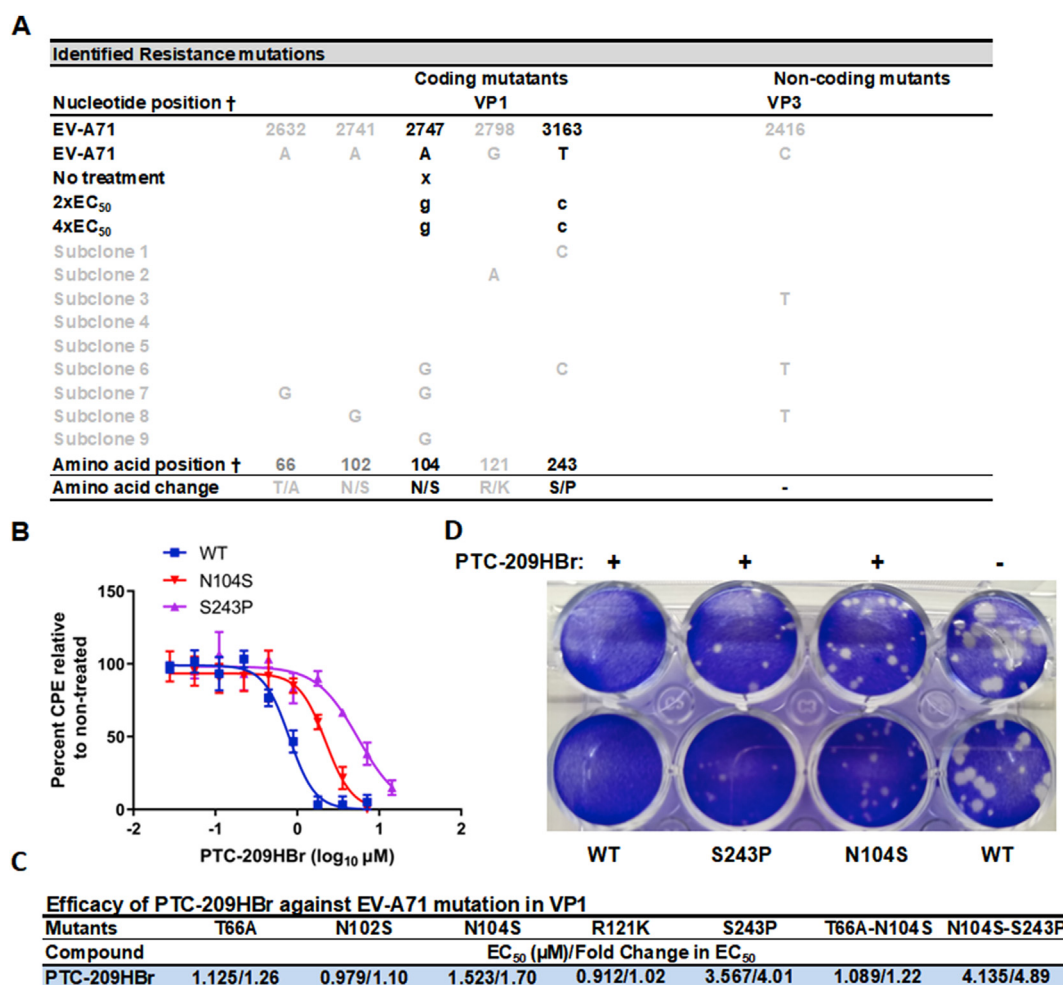


Fig. 3. Antiviral effect of PTC-209HBr and enviroxime against the selected specieses of *Enterovirus* (genus). (A, B) Concentration-response profiles used for EC<sub>50</sub> determination are shown for enterovirus inhibitors (A) PTC-209HBr and (B) enviroxime. Data points are means of triplicates SEM, for curve-fitting, described in Materials and Methods. One representative dataset of at least two independent experiments is shown. (C) EC<sub>50</sub>s of PTC-209HBr and enviroxime for selected enterovirus species were determined in short-term treatment assay by CPE (Materials and Methods). Representative EC<sub>50</sub> values from 2 to 3 independent experiments are given.



**Fig. 4. Selection of PTC-209HBr resistance and sensitivity to VP1 mutants.** (A) The PTC-209HBr resistance profiling. (B) The sensitivity of PTC-209HBr to VP1 mutant viruses, which was determined by a CPE assay. (C) EC<sub>50</sub>s of PTC-209HBr for VP1 mutant EV-A71 were determined in short-term treatment assay by CPE. (D) The sensitivity of PTC-209HBr to VP1 to PTC-209HBr at a concentration of 3.56 μM was determined by a plaque assay. For the plaque assay, RD cells were infected with EV-A71 or mutants at an MOI of  $2 \times 10^{-4}$ . For the CPE assay, RD cells were infected with EV-A71 at an MOI of 0.1.

was significant difference in binding affinity between the positive control pirodavir with VP1 and the N104S mutant (Fig. 5B). The MST assay results also showed that the enteroviral 3A inhibitor enviroxime had low binding affinity with VP1 (Fig. 5B). These data suggest that VP1 may directly bind to EV-A71 VP1 with robust affinity.

### 3.4. PTC-209HBr inhibits EV-A71 at the early infection stage

The potential target of PTC-209HBr was primarily identified by the resistance assay and MST assay. However, VP1 is a multifunctional protein participating in the viral life cycle, and the antiviral mechanism of PTC-209HBr needs to be further elucidated. To assess which stage of EV-A71 infection PTC-209HBr inhibited, a time-course assay was carried out in RD and Vero cells in the context of EV-A71 infection as previously reported. RD and Vero cells were infected with EV-A71 at an MOI of 0.1, followed by the initial treatment with PTC-209HBr (3.20 μM) and enviroxime (0.56 μM) or pirodavir (0.72 μM) at the indicated times following viral absorption (0, 1, 2, 4, 6, and 8 hpi). Cell lysates were collected at 12 hpi, and the viral structural protein VP1 and viral mRNA were quantified using a Western blot and qRT-PCR assay, respectively. The VP1 and viral RNA abundances were compared to those of the virus control (nontreated). In the presence of PTC-209HBr, inhibition rates at 0 and 1 h were close to 100% in RD cells (Fig. 6A, C) and Vero cells (Fig. 6A, C). Similar results were observed in the presence of pirodavir in

Vero cells and RD cells (Fig. 6B and C). However, enviroxime suppressed the accumulation of VP1 and mRNA at the four early time points in RD cells (Fig. 6A, C). The time-course assay results indicated that PTC-209HBr exerted antiviral effects during the early stages of EV-A71 infection.

### 3.5. PTC-209HBr blocks EV-A71 attachment and entry

PTC-209HBr has been identified with antiviral effects during the early stages of EV-A71 infection by a time-course experiment, however, the attachment or entry of EV-A71 whether impeded by PTC-209HBr are not clear. In order to elucidate the potential function affected by PTC-209HBr, binding and entry assays were conducted to illustrate the mode of action of PTC-209HBr. The results of binding and entry assays showed that PTC-209HBr could significantly inhibit the binding and entry process in dose-dependent manner (Fig. 7A and B) in RNA level. Pirodavir, a VP1 inhibitor, could dramatically inhibit EV-A71 binding but not entry (Fig. 7B and C). Enviroxime, a 3A inhibitor, little inhibited the EV-A71 binding and entry (Fig. 7B and C). The entry assay showed PTC-209HBr and pirodavir could robustly decrease the accumulation of VP1 expression (Fig. 7E). These data indicated that PTC-209HBr inhibited EV-A71 infection during the early stages of EV-A71 by blocking EV-A71 attachment and entry.

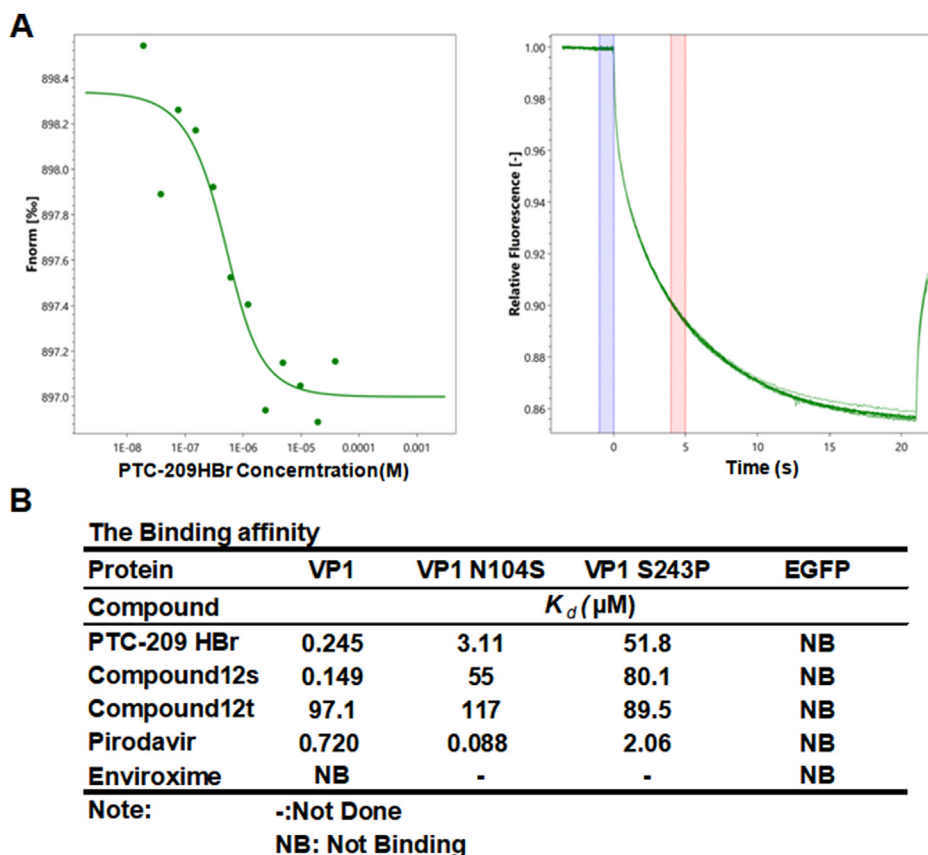


**Fig. 5. Binding affinities of PTC-209HBr, derivatives, pirodavir and enviroxime among VP1 or VP1 mutants were determined by MST.** (A) The change in fluorescence to thermophoresis at the increasing concentrations of PTC-209HBr (4.8–156000 nM) in the presence of 500 nM VP1-EGFP. (B) The binding affinities of PTC-209HBr, derivatives (12s, 12t), pirodavir and enviroxime among VP1 or VP1 mutants.

**3.6. PTC-209HBr impedes the interaction between VP1 and the receptor hSCARB2**

PSGL1 and hSCARB2 play critical roles in the early steps of EV-A71 infection and function as receptors of enteroviruses. Hsieh et al. identified that rosmarinic acid exerts antiviral effects by impeding the interaction between VP1 and cognate sulfated receptors and that the N104K mutation is an important determinant of rosmarinic acid resistance (Hsieh et al., 2020). Zhou et al. reported that the EV-A71 attachment complex, ‘A-particles’, is a variant of EV-A71 genotype B2 whose

infectivity is enhanced at low pH by a single mutation in VP1(N104S) (Dang et al., 2014). Interestingly, our results indicated that the N104S mutation also plays an important role in conferring PTC-209HBr resistance. Binding and entry assays indicated that PTC-209HBr exhibits antiviral activity by impeding virus binding and entry, which suggests that the binding site of PTC-209HBr may overlap with the binding sites of receptors. To investigate whether PTC-209HBr exerts its antiviral activity by blocking virus attachment to hSCARB2, an IF assay was carried out to determine colocalization between VP1 and hSCARB2 in the presence of PTC-209HBr. In line with our hypothesis, the colocalization between VP1

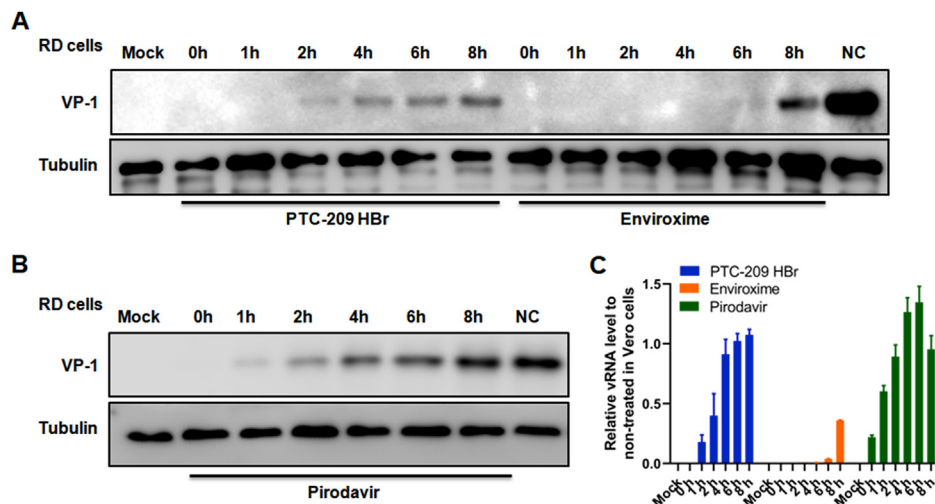


**Fig. 6. The action stage of PTC-209HBr, enviroxime and pirodavir was determined by a time-course assay.** PTC-209HBr, enviroxime and pirodavir at 1.78  $\mu$ M, 0.56  $\mu$ M and 0.72  $\mu$ M were added to the EV-A71-infected RD or Vero cells at the indicated time points. Samples were harvested at 12 hpi as described in the Materials and Methods. (A) Western blotting was carried out to assess the accumulation of VP1 expression in the presence of PTC-209HBr, enviroxime and pirodavir (A, B). The relative EV-A71 RNA levels in cells of the treated or untreated cases with PTC-209HBr, enviroxime and pirodavir were determined by qRT-PCR. One set of representative data out of at least two independent experiments with standard errors are showed.

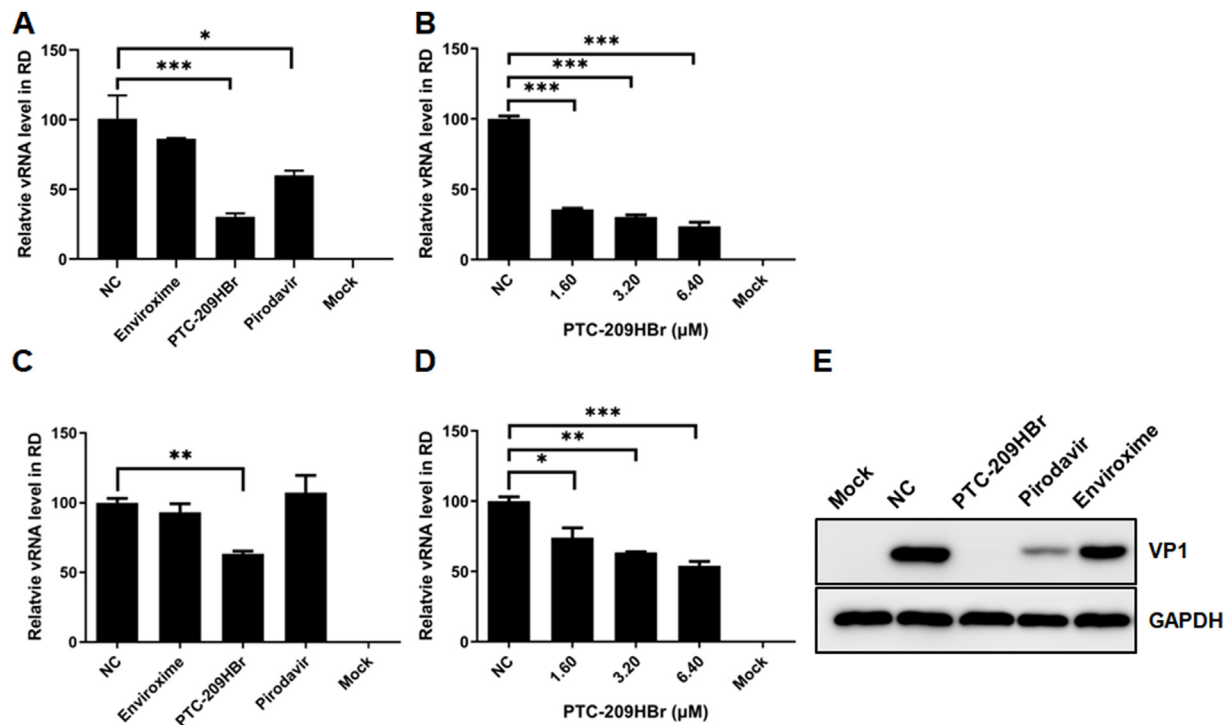


**Fig. 7. PTC-209HBr impedes EV-A71 binding and entry.** The binding and entry assays were quantitated by qRT-PCR or Western blot. PTC-209HBr, enviroxime and pirodavir at specific concentration were added to the EV-A71-infected RD or Vero cells at the indicated time points. Samples were harvested at indicated time points as described in the Materials and Methods. (A) qRT-PCR was carried out to assess relative EV-A71 RNA levels in cells of the treated or untreated cases with PTC-209HBr (3.2 μM), enviroxime (0.32 μM) and pirodavir (0.64 μM) during the binding stage. (B) PTC-209HBr decreased EV-A71 infection in a dose-independent manner during the binding stage. (C) qRT-PCR was carried out to assess relative EV-A71 RNA levels in cells of the treated or untreated cases with PTC-209HBr (3.2 μM), enviroxime (0.32 μM) and pirodavir (0.64 μM) during the entry stage. (D) PTC-209HBr dose-dependently decreased EV-A71 infection during the entry stage. (E) The accumulation of VP1 expression in the presence of PTC-209HBr, enviroxime and pirodavir was analyzed by a Western blot assay during the binding stage. One set of representative data out of at least two independent experiments with standard errors are showed.

and hSCARB2 in EV-A71-infected cells was dramatically reduced in cells treated with PTC-209HBr compared to untreated cells and was also decreased in cells treated with enviroxime since it exerts antiviral activity at the internalization (entry) step (Fig. 8A). The Co-IP assay results showed that the interaction between VP1 and hSCARB2 was also inhibited by PTC-209HBr (Fig. 8B). These results indicated that PTC-209HBr exerts antiviral activity by impeding the interaction between EV-A71 and the receptor.

### 3.7. N104S enhances the interaction between VP1 and hSCARB2 in the presence of PTC-209HBr

The MST assay indicated that residues VP1 N104 and S243 may be the binding site of PTC-209HBr. Although Zhou et al. has reported that the EV-A71 attachment complex, 'A-particles', is a variant of EV-A71 genotype B2 whose infectivity is enhanced at low pH by a single mutation in VP1(N104S) (Dang et al., 2014). However, the mechanism of these two mutants in EV-A71 resistance and fitness is unclear. To elucidate the molecular mechanism of antivirals and the evolutionary pathways to persistence of highly fit and resistant enterovirus capsid inhibitors, an IF assay was carried out to investigate the colocalization between mutant VP1 and hSCARB2. The IF assay showed that the VP1 S243P variant did change the colocalization between VP1 and hSCARB2 in the presence of PTC-209HBr compared to that in the presence of DMSO (Fig. 9). However, N104S did not impede the colocalization between VP1 and hSCARB2 in the presence of PTC-209HBr compared to that in the presence of DMSO (Fig. 9). These data indicated that N104S may increase fitness by enhancing the interaction between VP1 and hSCARB2 in the presence of PTC-209HBr but not S243P.

### 3.8. Proposed docking position of PTC-209HBr with EV-A71 VP1 protein

As the VP1 N104 and S243 residues may be the targets of PTC-209HBr, PTC-209HBr was docked onto the constraint area, which encompasses these residues. The results revealed a potential binding site surrounding the cluster of N102, N104, R121 and S243 in the PTC-209HBr model (Fig. 10B); PTC-209HBr may interact with N102, N104, R166, L242, S243, and L97 of the parental VP1 protein in the docking model (Fig. 10A). And PTC-209HBr may bind to the N104 via hydrogen bonds in the docking model of N104 VP1 protein (Fig. 10A). The docking position of PTC-209HBr, however, is distant from the fivefold axis. We further analyzed the VP1 sequence of different EV-A71 viruses, which have been classified into genotypes A, B, and C based on the VP1 sequence. These results showed that N104 and N102 are highly conserved (sFig. 3), suggesting that PTC-209HBr has broad targeting potential against EV-A71 infection, which was confirmed in an inhibition spectrum assay (Fig. 3).

## 4. Discussion

The first step in successful enteroviral infection and one of the key determinants of viral tropism and pathogenesis is the binding between the host cell receptor and capsid protein involved in the recognition of receptors on host cell surface. Different enteroviruses also have distinct attachment and uncoating receptors, which provides a possible explanation for the different diseases caused by enteroviruses. In addition, the adsorption receptors and uncoating receptors used by enteroviruses differ across tissues. For example, the adsorption receptors of EV-A71 have been reported to include hSCARB2, PSGL1, Annexin II, heparan sulfate and sialic acid. The differential expression of these receptors in different tissues or cells may also explain the viral tropism of EV-A71.

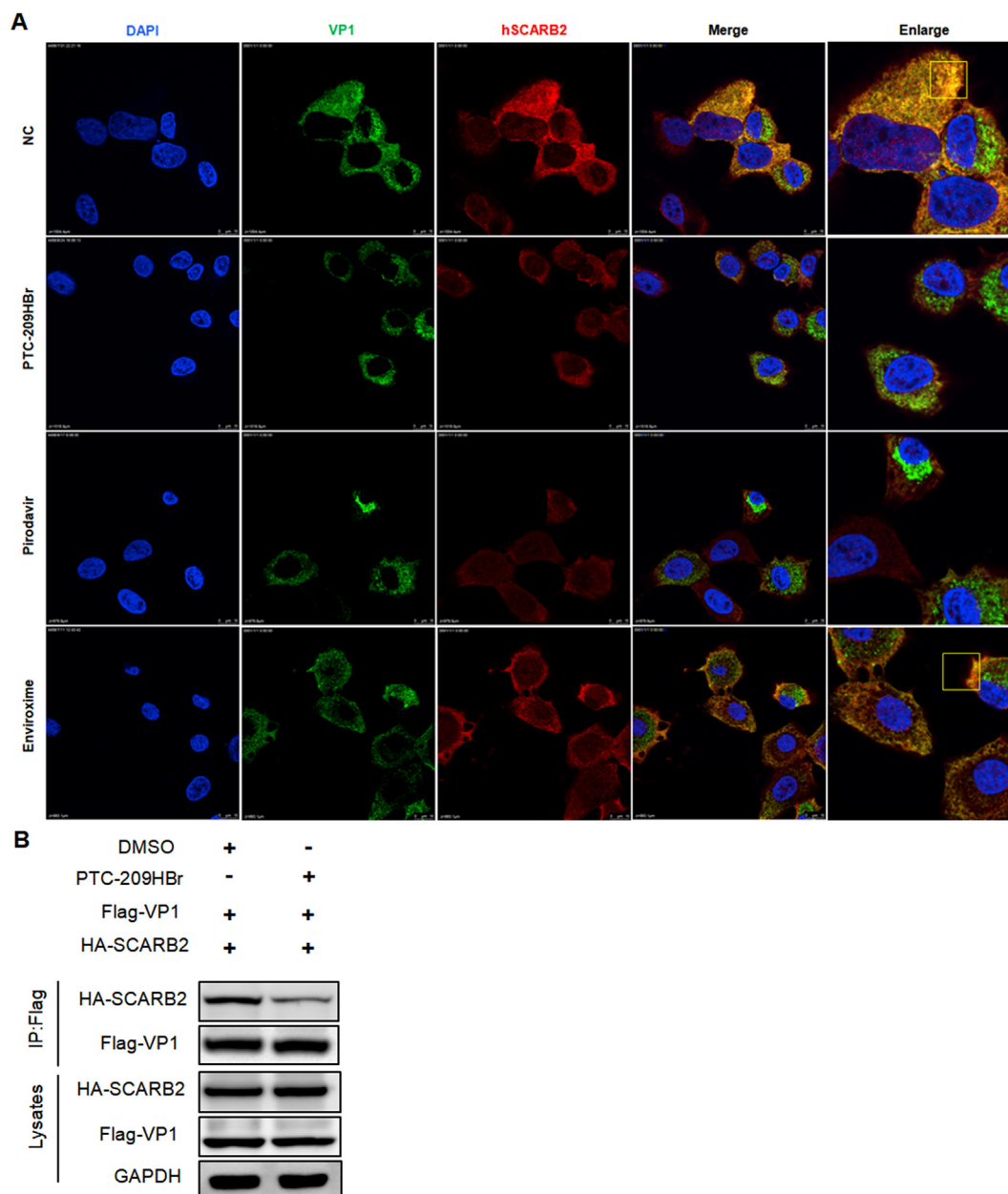


**Fig. 8. Colocalization of EV-A71 VP1 and hSCARB2 in the presence of PTC-209HBr, enviroxime and pirodavisir.** (A) The colocalization of EV-A71 VP1 and hSCARB2 in the presence of PTC-209HBr, enviroxime or pirodavisir. The yellow square indicates the colocalization of EV-A71 VP1 and hSCARB2. EV-A71 was mixed with the indicated concentration of PTC-209HBr and then incubated at 37 °C for 1 h. Then, the mixtures were incubated with RD cells at 4 °C for 1 h, washed with cold PBS three times, fixed with 10% formaldehyde solution and further subjected to IF analysis. These data were acquired from at least two independent assays. (B) Inhibition of the interaction between VP1 and hSCARB2 by PTC-209HBr was analyzed by Co-IP. HEK293T cells were co-transfected with Flag-VP1 and HA-hSCARB2, followed by the treatment of PTC-209HBr or DMSO at 24h post transfection. Cell lysates were immunoprecipitated with an anti-Flag antibody and were then analyzed by a Western blot assay.

Although there are many kinds of viral receptors, the processes of enterovirus uncoating and attachment are very conserved, so the pathway of viral capsid proteins binding to receptors is a potential drug target and has been widely studied. However, the research and development of enterovirus capsids and receptor inhibitors have lagged behind. In this study, we first identified PTC-209HBr (PTC-209), a small-molecule Bmi-1 inhibitor and an anticancer agent, as a VP1 inhibitor with broad-spectrum antiviral activity. PTC-209HBr was found to inhibit the proliferation of EV71/HeN09, EV71/G082, EV-D68, Echov-6, CV-A16 and CV-B3 with EC<sub>50</sub> values between 0.79 and 2.92 μM (Fig. 3B), suggesting that it has the potential to be developed as a broad-spectrum antiviral drug to treat enteroviral infections.

The possible mechanism of PTC-209HBr inhibition of enteroviruses could be the hindrance of enteroviral entry by impeding the interaction between VP1 and hSCARB2 (Fig. 11) (Zhou et al., 2019). To better investigate the potential mechanism of action of PTC-209HBr, a resistance assay was conducted to identify the interactions between PTC-209HBr and viral proteins. Amino acids T66A, N102S, N104S, R121K and S243P were identified in the escaped viruses by subclone assay. N102S showed slight resistance to PTC-209HBr, and only the mutant N104S and S243P viruses were sensitive to PTC-209HBr (Fig. 4C). These data indicated that VP1 is a potential target of PTC-209HBr in anti-enterovirus infection and that N104 and S243 are the main interaction sites of PTC-209HBr. To investigate whether

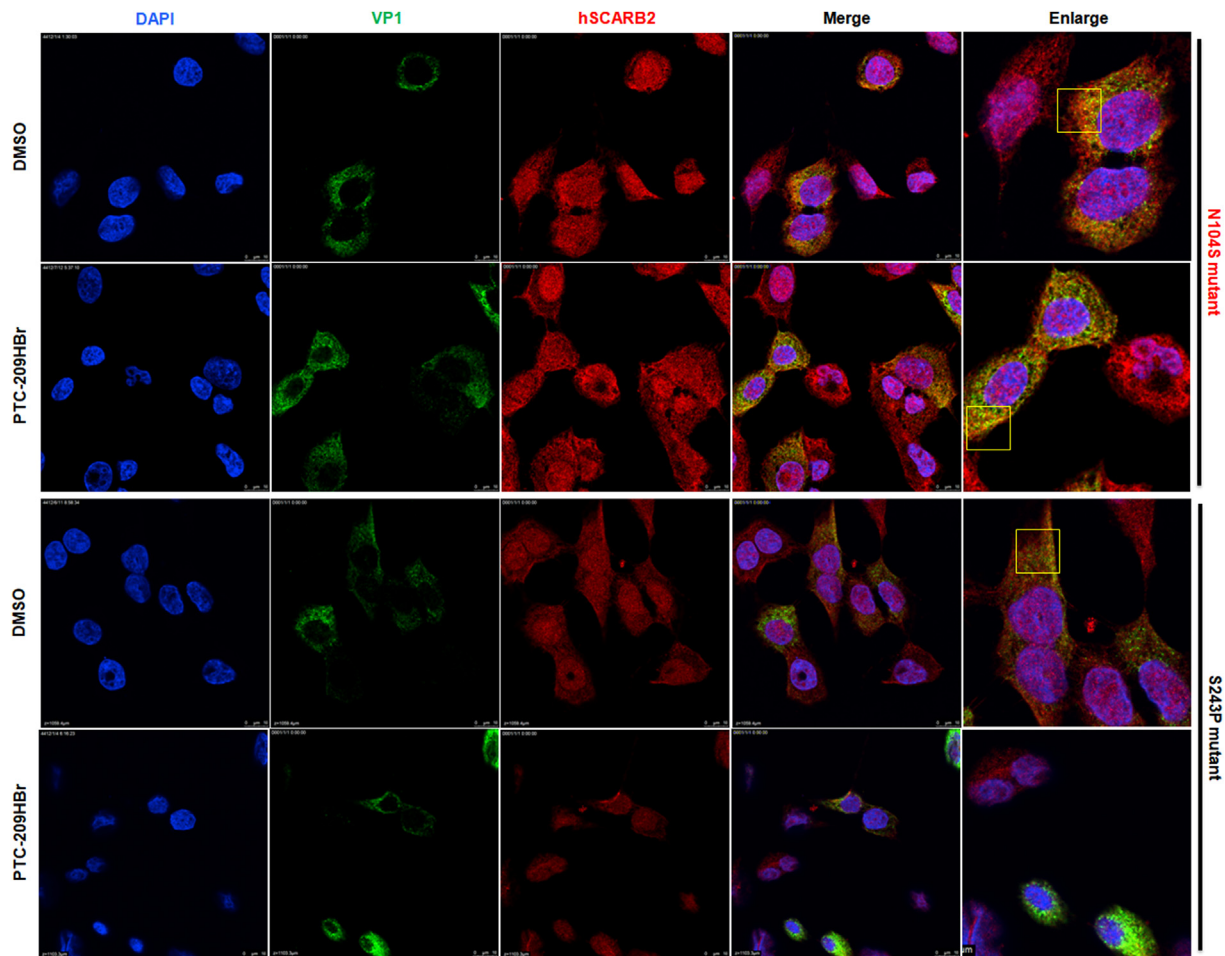


**Fig. 9.** Colocalization of EV-A71 variants and hSCARB2 in the treatment of PTC-209HBr or DMSO. The yellow square indicates the colocalization of VP1 and hSCARB2. EV-A71 was mixed with the indicated concentration of PTC-209HBr and then incubated at 37 °C for 1 h, followed by incubation with RD cells at 37 °C for 1 h. The treated cells were washed with cold PBS five times and then incubated at 37 °C and 5% CO<sub>2</sub> for 6 h. Cells were fixed at 6 hpi and then analyzed by IF. These data were acquired from at least two independent assays.

PTC-209HBr interacts with VP1 directly, a MST assay was carried out to test the binding affinity between VP1 and PTC-209HBr. The binding affinity value of EV-A71 VP1 with PTC-209HBr was 0.245  $\mu$ M. In line with the resistance results, the binding affinities ( $K_d$ ) of PTC-209HBr with mutant VP1 N104S and S243P were 3.11  $\mu$ M and 51.8  $\mu$ M, respectively. These data suggest that VP1 may directly bind to EV-A71 VP1 with robust affinity. Furthermore, the S243P mutation in EV-A71 VP1 not only significantly decreased viral fitness but also conferred resistance (data not shown), and the N104S mutation in EV-A71 VP1 conferred moderate resistance. However, VP1 is a multifunctional protein participating in the viral life cycle, and the antiviral mechanism of PTC-209HBr needs to be further elucidated. The time-course assay results indicated that PTC-209HBr exerted antiviral effects during the immediately early stages of EV-A71 infection and also exerted some antiviral activity at post-entry stage. These data indicated that PTC-209HBr may exert anti-EV-A71 effect by inhibition the replication of EV-A71. Bmi-1, a target of PTC-209HBr, regulating the replication of enteroviruses is seldom reported, thus whether EV-A71 depends on the pathway of BMI-1 needs further study.

Recently, the cocrystal structure of mature EV-A71 particles with hSCARB2 revealed that the VP1 GH loop is a mostly solvent-exposed region at the surface of the virus particle and binds with hSCARB2, which can mediate both attachment to the host cell and uncoating. The docking model of the crystal structures of EV-A71 and hSCARB2 showed that N104 is adjacent to the GH loop of VP1, which is predicted to be an

hSCARB2 binding site. Interestingly, N102S and N104S were further identified in the escaped viruses by a subclone assay. We speculated that PTC-209HBr may impede the interaction between VP1 and hSCARB2. In line with our hypothesis, IF and Co-IP assays showed that PTC-209HBr could significantly decrease the interaction between VP1 and hSCARB2, and N104S could enhance the binding between VP1 and hSCARB2 in the presence of PTC-209HBr. This evidence indicated that PTC-209HBr may hinder enteroviral entry by impeding the interaction between VP1 and hSCARB2.

VP1 N104 and S243 have been a hotspot in the development of enteroviral capsid inhibitors. Qing et al. reported that the site of the acid-resistance mutation N104S, is adjacent to the GH loop which has been shown to be a cyclophilin A interaction site (S243, P246), meaning that N104 is present in an area that is involved in cyclophilin A interactions. Interestingly, we also observed that the S243P mutant showed resistance to PTC-209HBr, and the binding affinity of PTC-209HBr to S243P VP1 was dramatically lower than that of WT VP1. Therefore, whether PTC-209HBr impedes the binding between cyclophilin A and VP1, thus blocking enterovirus uncoating, needs to be further investigated.

The emergence of resistant viruses and virus strains with intra- or intertypic recombination has been the main challenge in improving the efficacy of therapeutics or vaccines. The possibility for this involves the natural ability of RNA viruses to rapidly develop resistance that is dependent on RNA replicases and transcriptases associated with the absence or low efficiency of proofreading repair activities (Sanjuan and

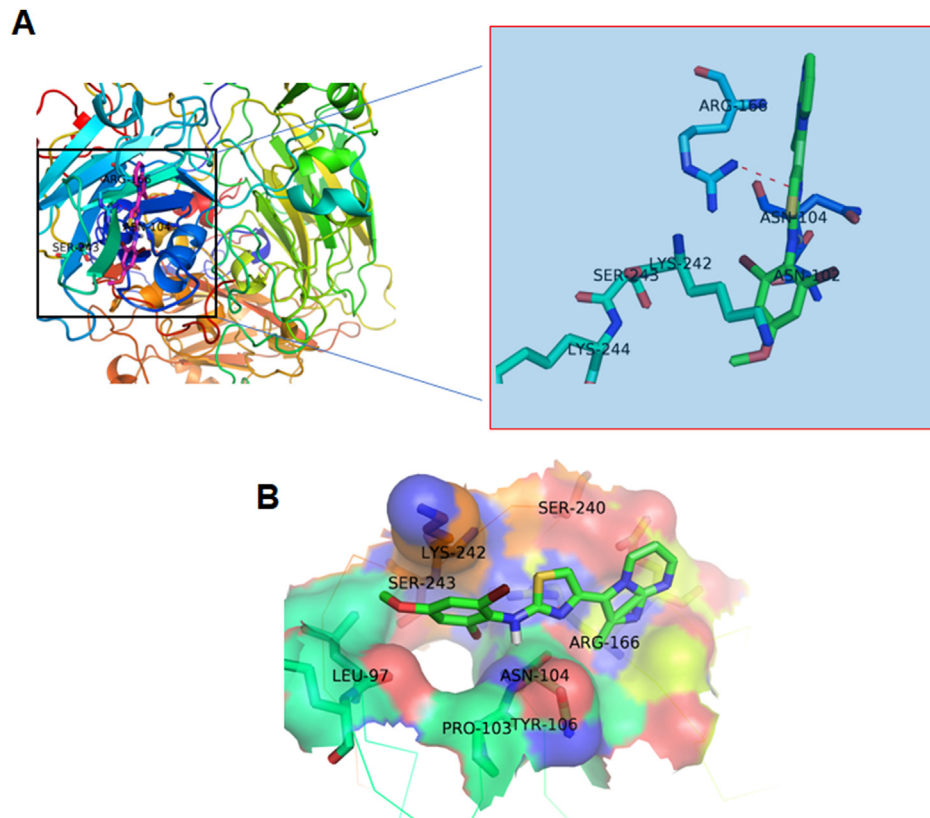


**Fig. 10. Proposed docking model of PTC-209HBr with EV-A71 VP1 protein.** (A) Molecular docking model of the binding between PTC-209HBr and EV-A71 capsid protein VP1. (B) The predicted amino acid residues may bind with PTC-209HBr or be related to resistance to TC-209HBr. The hydrogen bond is shown as a red dotted line, and some hydrophobic amino acids within 5 Å are labeled. The oxygen atom (red), nitrogen atom (blue) and sulfur atom (yellow) are also shown.

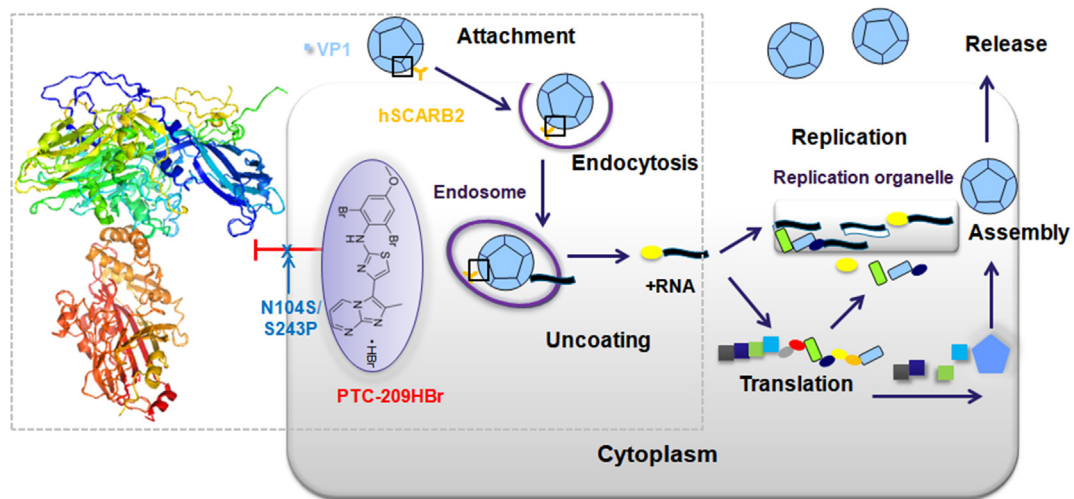


**Fig. 11. The proposed model of PTC-209HBr inhibition of EV-A71.** The model of the interaction between hSCARB2 and EV71 protomer as previously reported (Zhou et al., 2019). VP1, VP2, VP3, VP4 and hSCARB2 are coloured in blue, green, red, yellow and orange, respectively.

Domingo-Calap, 2016). The sequence alignment results indicated that the VP1 N104 residue is highly conserved and present in various enteroviruses. The VP1 S243 residue is conserved in only some enteroviruses, such as EV-A71 and CV-A16 (sFig. 3). In line with the alignment results, PTC-209HBr exerts potential antiviral activities against EV71/HeN09, EV71/G082, EV-D68, Echov-6, CV-A16 and CV-B3 (Fig. 3). Therefore, PTC-209HBr may be useful for the treatment of emerging enterovirus variants.

In conclusion, we initially identified PTC-209HBr as a panenterovirus inhibitor due to its ability to inhibit the interaction between hSCARB2 and VP1 by targeting VP1 with  $EC_{50}$  values between 0.79 and 2.92  $\mu$ M. Our studies on the mechanism of action, drug resistance and fitness have been carried out to elucidate the molecular mechanism of antivirals, and the evolutionary pathways of fit and resistant enterovirus inhibitor escape variants provide insights into the molecular mechanism of virus-host interactions and antiviral research systems.

## Author disclosure statement

The authors declare no competing financial interest.

## Acknowledgments

We thank Dr Bo Zhang (Wuhan, China) for pACYC-EV71-FL, and Dr Tao Peng (Guangzhou, China) and Dr Zhong Huang (Shanghai, China) for EV-A71 GZ-CII mouse adapted virus and EV71/G082, respectively. This research is supported by the NSFC (32188101, 82102374, 81971976, 81772236).

## Appendix A. Supplementary data

Supplementary data to this article can be found online at <https://doi.org/10.1016/j.cellin.2022.100016>.

## References

- Anasir, M. I., Zarif, F., & Poh, C. L. (2021). Antivirals blocking entry of enteroviruses and therapeutic potential. *J. Biomed. Sci.*, *28*, 10.
- Baer, A., & Kehn-Hall, K. (2014). Viral concentration determination through plaque assays: using traditional and novel overlay systems. *JoVE*, Article e52065.
- Baggen, J., Thibaut, H. J., Strating, J., & van Kuppeveld, F. J. M. (2018). The life cycle of non-polio enteroviruses and how to target it. *Nat. Rev. Microbiol.*, *16*, 368–381.
- Chang, L. Y., Lin, T. Y., Hsu, K. H., Huang, Y. C., Lin, K. L., Hsueh, C., Shih, S. R., Ning, H. C., Hwang, M. S., Wang, H. S., et al. (1999). Clinical features and risk factors of pulmonary oedema after enterovirus-71-related hand, foot, and mouth disease. *Lancet*, *354*, 1682–1686.
- Chong, P., Liu, C. C., Chow, Y. H., Chou, A. H., & Klein, M. (2015). Review of enterovirus 71 vaccines. *Clin. Infect. Dis.*, *60*, 797–803.
- Dang, M., Wang, X., Wang, Q., Wang, Y., Lin, J., Sun, Y., Li, X., Zhang, L., Lou, Z., Wang, J., et al. (2014). Molecular mechanism of SCARB2-mediated attachment and uncoating of EV71. *Protein Cell*, *5*, 692–703.
- Entzian, C., & Schubert, T. (2016). Studying small molecule–aptamer interactions using MicroScale Thermophoresis (MST). *Methods*, *97*, 27–34.
- Fleischer, R., & Laessig, K. (2003). Safety and efficacy evaluation of pleconaril for treatment of the common cold. *Clin. Infect. Dis.*, *37*, 1722.
- Gunaseelan, S., Wong, K. Z., Min, N., Sun, J., Ismail, N., Tan, Y. J., Lee, R. C. H., & Chu, J. J. H. (2019). Prunin suppresses viral IRES activity and is a potential candidate for treating enterovirus A71 infection. *Sci. Transl. Med.*, *11*.
- Han, X., Sun, N., Wu, H., Guo, D., Tien, P., Dong, C., Wu, S., & Zhou, H. B. (2016). Identification and structure-activity relationships of diarylhydrazides as novel potent and selective human enterovirus inhibitors. *J. Med. Chem.*, *59*, 2139–2150.
- Hopcraft, S. E., Pattenden, S. G., James, L. I., Frye, S., Dittmer, D. P., & Damania, B. (2018). Chromatin remodeling controls Kaposi's sarcoma-associated herpesvirus reactivation from latency. *PLoS Pathog.*, *14*, Article e1007267.
- Hsieh, C. F., Jheng, J. R., Lin, G. H., Chen, Y. L., Ho, J. Y., Liu, C. J., Hsu, K. Y., Chen, Y. S., Chan, Y. F., Yu, H. M., et al. (2020). Rosmarinic acid exhibits broad anti-enterovirus A71 activity by inhibiting the interaction between the five-fold axis of capsid VP1 and cognate sulfated receptors. *Emerg. Microb. Infect.*, *9*, 1194–1205.
- Hu, Y., Musharrafieh, R., Zheng, M., & Wang, J. (2020). Enterovirus D68 antivirals: past, present, and future. *ACS Infect. Dis.*, *6*, 1572–1586.
- Huang, S. W., Hsu, Y. W., Smith, D. J., Kiang, D., Tsai, H. P., Lin, K. H., Wang, S. M., Liu, C. C., Su, I. J., & Wang, J. R. (2009). Reemergence of enterovirus 71 in 2008 in Taiwan: dynamics of genetic and antigenic evolution from 1998 to 2008. *J. Clin. Microbiol.*, *47*, 3653–3662.
- Jensen, S. B., Fahnøe, U., Pham, L. V., Serre, S. B. N., Tang, Q., Ghanem, L., Pedersen, M. S., Ramirez, S., Humes, D., Pihl, A. F., et al. (2019). Evolutionary pathways to persistence of highly fit and resistant Hepatitis C virus protease inhibitor escape variants. *Hepatology*, *70*, 771–787.
- Kang, H., Kim, C., Kim, D. E., Song, J. H., Choi, M., Choi, K., Kang, M., Lee, K., Kim, H. S., Shin, J. S., et al. (2015). Synergistic antiviral activity of gemcitabine and ribavirin against enteroviruses. *Antivir. Res.*, *124*, 1–10.
- Lee, K. M., Chen, C. J., & Shih, S. R. (2017). Regulation mechanisms of viral IRES-driven translation. *Trends Microbiol.*, *25*, 546–561.
- Lin, J.-Y., Kung, Y.-A., & Shih, S.-R. (2019). Antivirals and vaccines for enterovirus A71. *J. Biomed. Sci.*, *26*, 65.
- Linsuwanon, P., Puenpa, J., Huang, S. W., Wang, Y. F., Mauleekoonphairoj, J., Wang, J. R., & Poovorawan, Y. (2014). Epidemiology and seroepidemiology of human enterovirus 71 among Thai populations. *J. Biomed. Sci.*, *21*, 16.
- Lou, Z., Sun, Y., & Rao, Z. (2014). Current progress in antiviral strategies. *Trends Pharmacol. Sci.*, *35*, 86–102.
- Osterback, R., Vuorinen, T., Linna, M., Susi, P., Hyypiä, T., & Waris, M. (2009). Coxsackievirus A6 and hand, foot, and mouth disease, Finland. *Emerg. Infect. Dis.*, *15*, 1485–1488.
- Pham, L. V., Jensen, S. B., Fahnøe, U., Pedersen, M. S., Tang, Q., Ghanem, L., Ramirez, S., Humes, D., Serre, S. B. N., Schönning, K., et al. (2019). HCV genotype 1-6 NS3 residue 80 substitutions impact protease inhibitor activity and promote viral escape. *J. Hepatol.*, *70*, 388–397.
- Plevka, P., Perera, R., Cardoso, J., Kuhn, R. J., & Rossmann, M. G. (2012). Crystal structure of human enterovirus 71. *Science*, *336*, 1274.
- Rossmann, M. G., He, Y., & Kuhn, R. J. (2002). Picornavirus-receptor interactions. *Trends Microbiol.*, *10*, 324–331.
- Sanjuan, R., & Domingo-Calap, P. (2016). Mechanisms of viral mutation. *Cell. Mol. Life Sci.*, *73*, 4433–4448.
- Shang, B., Deng, C., Ye, H., Xu, W., Yuan, Z., Shi, P. Y., & Zhang, B. (2013). Development and characterization of a stable eGFP enterovirus 71 for antiviral screening. *Antivir. Res.*, *97*, 198–205.
- Shia, K. S., Li, W. T., Chang, C. M., Hsu, M. C., Chern, J. H., Leong, M. K., Tseng, S. N., Lee, C. C., Lee, Y. C., Chen, S. J., et al. (2002). Design, synthesis, and structure-activity relationship of pyridyl imidazolidinones: a novel class of potent and selective human enterovirus 71 inhibitors. *J. Med. Chem.*, *45*, 1644–1655.
- Solomon, T., Lewthwaite, P., Perera, D., Cardoso, M. J., McMinn, P., & Ooi, M. H. (2010). Virology, epidemiology, pathogenesis, and control of enterovirus 71. *Lancet Infect. Dis.*, *10*, 778–790.
- Sun, L., Lee, H., Thibaut, H. J., Lanko, K., Rivero-Buceta, E., Bator, C., Martinez-Gualda, B., Dallmeier, K., Delang, L., Leyssen, P., et al. (2019). Viral engagement with host receptors blocked by a novel class of tryptophan dendrimers that targets the 5-fold-axis of the enterovirus-A71 capsid. *PLoS Pathog.*, *15*, Article e1007760.
- Tang, Q., Li, S., Du, L., Chen, S., Gao, J., Cai, Y., Xu, Z., Zhao, Z., Lan, K., & Wu, S. (2020a). Emetine protects mice from enterovirus infection by inhibiting viral translation. *Antivir. Res.*, *173*, 104650.
- Tang, Q., Wu, Y. Q., Chen, D. S., Zhou, Q., Chen, H. C., & Liu, Z. F. (2014). Bovine herpesvirus 5 encodes a unique pattern of microRNAs compared with bovine herpesvirus 1. *J. Gen. Virol.*, *95*, 671–678.
- Tang, Q., Xu, Z., Jin, M., Shu, T., Chen, Y., Feng, L., Zhang, Q., Lan, K., Wu, S., & Zhou, H. B. (2020b). Identification of dibucaine derivatives as novel potent enterovirus 2C helicase inhibitors: in vitro, in vivo, and combination therapy study. *Eur. J. Med. Chem.*, *202*, 112310.
- Tijmsma, A., Franco, D., Tucker, S., Hilgenfeld, R., Froeyen, M., Leyssen, P., & Neyts, J. (2014). The capsid binder Vapendavir and the novel protease inhibitor SG85 inhibit enterovirus 71 replication. *Antimicrob. Agents Chemother.*, *58*, 6990–6992.
- Tosteson, M. T., & Chow, M. (1997). Characterization of the ion channels formed by poliovirus in planar lipid membranes. *J. Virol.*, *71*, 507–511.
- Wang, J., Hu, Y., & Zheng, M. (2021). Enterovirus A71 antivirals: past, present, and future. *Acta Pharm. Sin. B*. <https://doi.org/10.1016/j.apbsb.2021.08.017>. In press.
- Wen, W., Li, X., Yin, M., Wang, H., Qin, L., Li, H., Liu, W., Zhao, Z., Zhao, Q., Chen, H., et al. (2021). Selective autophagy receptor SQSTM1/p62 inhibits Seneca Valley virus replication by targeting viral VP1 and VP3. *Autophagy*, 1–13.
- Wu, Y., Yeo, A., Phoon, M. C., Tan, E. L., Poh, C. L., Quak, S. H., & Chow, V. T. (2010). The largest outbreak of hand, foot and mouth disease in Singapore in 2008: the role of enterovirus 71 and coxsackievirus A strains. *Int. J. Infect. Dis.*, *14*, e1076–1081.
- Xia, H., Wang, P., Wang, G. C., Yang, J., Sun, X., Wu, W., Qiu, Y., Shu, T., Zhao, X., Yin, L., et al. (2015). Human enterovirus nonstructural protein 2CATPase functions as both an RNA helicase and ATP-independent RNA chaperone. *PLoS Pathog.*, *11*, Article e1005067.
- Xing, W., Liao, Q., Viboud, C., Zhang, J., Sun, J., Wu, J. T., Chang, Z., Liu, F., Fang, V. J., Zheng, Y., et al. (2014). Hand, foot, and mouth disease in China, 2008–12: an epidemiological study. *Lancet Infect. Dis.*, *14*, 308–318.
- Xu, Y., Ma, S., Zhu, L., Huang, Z., Chen, L., Xu, Y., Yin, H., Peng, T., & Wang, Y. (2017). Clinically isolated enterovirus A71 subgenogroup C4 strain with lethal pathogenicity in 14-day-old mice and the application as an EV-A71 mouse infection model. *Antivir. Res.*, *137*, 67–75.
- Yang, B., Liu, F., Liao, Q., Wu, P., Chang, Z., Huang, J., Long, L., Luo, L., Li, Y., Leung, G. M., et al. (2017). Epidemiology of hand, foot and mouth disease in China, 2008 to 2015 prior to the introduction of EV-A71 vaccine. *Euro Surveill.*, *22*.
- Yu, Y., Tang, Q., Xu, Z., Li, S., Jin, M., Zhao, Z., Dong, C., Wu, S., & Zhou, H. B. (2018). Synthesis and structure-activity relationship study of arylsulfonamides as novel potent H5N1 inhibitors. *Eur. J. Med. Chem.*, *159*, 206–216.
- Zeng, M., El Khatib, N. F., Tu, S., Ren, P., Xu, S., Zhu, Q., Mo, X., Pu, D., Wang, X., & Altmeyer, R. (2012). Seroepidemiology of Enterovirus 71 infection prior to the 2011 season in children in Shanghai. *J. Clin. Virol.*, *53*, 285–289.
- Zhou, D., Zhao, Y., Kotecha, A., Fry, E. E., Kelly, J. T., Wang, X., Rao, Z., Rowlands, D. J., Ren, J., & Stuart, D. I. (2019). Unexpected mode of engagement between enterovirus 71 and its receptor SCARB2. *Nat. Microbiol.*, *4*, 414–419.